Micromagnetic simulation of domain wall dynamics in Permalloy nanotubes at high frequencies

I. Betancourt,[a] G. Hrkac, and T. Schrefl
Department of Engineering Materials, University of Sheffield, Sir Robert Hadfield Bldg., Mappin Street, Sheffield, S1 3JD, United Kingdom

(Received 18 February 2008; accepted 21 May 2008; published online 28 July 2008)

The formation and motion of a single cross-tie type domain wall (DW) was studied in a $Ni_{80}Fe_{20}$ Permalloy nanotube of 50 nm thickness and 500 nm length by means of micromagnetic simulations. Circular magnetization curves, calculated with circumferential ac magnetic fields applied on the nanotube, showed that the propagation of the DW along the nanotube length occurred for h_{rms} values as low as 166 A/m at a frequency of 250 MHz. In general, the observed DW motion exhibited an out-of-phase oscillating character, relative to the applied h_{ac} field, with a normalized phase shift of 0.20 being independent of h_{rms}. The DW damping was observed at 10 GHz. © *2008 American Institute of Physics*. [DOI: 10.1063/1.2960480]

I. INTRODUCTION

The interaction between microwaves and magnetic materials is becoming an area of increasing interest associated with the development of micro- and nanodevices such as power conversion circuits (including inductors and transformers), integrated radio-frequency passive components, micromagnetic devices, and microwave-assisted recording,[1–5] for which a basic understanding of the dynamics of the magnetization reversal processes in the magnetic nanostructures is of great relevance for technological improvements of such nanodevices operating within the gigahertz range.[4,5] In particular, magnetic domain wall (DW) motion in nanostructures has deserved recent attention because of their potential use in magnetic devices for information transport.[6–8] For instance, it has been shown experimentally that a DW confined within a pining potential of a Permalloy nanowire can be manipulated with a spin polarized electric current, which allows DW motion for threshold magnetic field values within the range 5–10 Oe.[9] Resonant amplification of DW oscillations has also been observed.[10]

Concerning magnetic nanotubes, previous analytical/numerical simulation work has shown that their static magnetization distribution is strongly dependent on the nanotube geometry. There are three possible magnetization distributions: perpendicular to the nanotube main axis, parallel to main axis, and vortex state, for which magnetization along circular direction develops.[11,12] In addition, anisotropic magnetoresistance has been also predicted in Ni–Fe nanotubes.[11] Nevertheless, no attention has been focused so far on the magnetic DW response to time dependent magnetic fields of variable magnitude. In this work, we present a systematic study by means of micromagnetic simulations of the DW dynamics in a $Ni_{80}Fe_{20}$ Permalloy nanotube as a function of both frequency (within the range 250 MHz—10 GHz.) and intensity of ac magnetic fields.

II. SIMULATION METHOD

Micromagnetic simulations have been carried out as follows. The dynamic magnetization process in the nanotube is described by the Landau–Lifshitz–Gilbert (LLG) equation of motion

$$\frac{\partial \mathbf{M}}{\partial t} = -\gamma' \mathbf{M} \times \mathbf{H}_{\text{eff}} - \frac{\alpha \gamma'}{M_s} \mathbf{M} \times (\mathbf{M} \times \mathbf{H}_{\text{eff}}), \tag{1}$$

where $\gamma' = \gamma/(1+\alpha^2)$, α is a dimensionless damping constant, and γ is the electron gyromagnetic ratio. The effective field $\mathbf{H}_{\text{eff}}$ is composed of the anisotropy field $\mathbf{H}_{\text{ani}}$, the exchange contribution $\mathbf{H}_{\text{exch}}$, the applied field $\mathbf{H}_a$, and the magnetostatic field $\mathbf{H}_M$.[13] The contributing fields are calculated from Maxwell equations.[14] Here the applied field is the Oersted field that is generated by a current carrier model consisting of a cylinder symmetrically located inside the Permalloy nanotube. The field is calculated using the Biot–Savart law,

$$\mathbf{H}_a(\mathbf{r}) = \frac{1}{4\pi} \int_V \mathbf{j} \times \frac{\mathbf{r} - \mathbf{r}'}{|\mathbf{r} - \mathbf{r}'|^3} dV', \tag{2}$$

as described in Ref. 15. The integral in Eq. (2) is over the volume of the conductor. The cylinder is discretized into tetrahedral finite elements. Under the assumption that the current density is constant in each tetrahedron, Eq. (2) can be written as sum over surface integrals,[16]

$$\mathbf{H}_a(\mathbf{r}) = \sum_{e=1}^{N} \mathbf{j}_e \times \sum_{e_i=1}^{4} \frac{1}{4\pi} \int \frac{1}{|\mathbf{r} - \mathbf{r}'|} d\mathbf{A}'. \tag{3}$$

The first sum in Eq. (3) is over all tetrahedrons of the conductor, the second sum is over all triangles of a tetrahedron. The integrals in Eq. (3) are evaluated analytically.[17] On the other hand, the magnetostatic field $\mathbf{H}_M$ is an irrotational

[a]Author to whom correspondence should be addressed. On a sabbatical leave from Departamento de Materiales Metalicos y Ceramicos, Instituto de Investigaciones en Materiales, Universidad Nacional Autonoma de Mexico, Mexico D.F. 04510, Mexico. Electronic mail: israelb@correo.unam.mx.

field and is calculated by applying the magnetostatic potential u_M into the following conditional Maxwell equations:

$$\nabla \cdot \mathbf{H}_M = -\nabla \cdot \mathbf{M}, \tag{4}$$

$$\nabla \times \mathbf{H}_M = 0, \tag{5}$$

$$\nabla \cdot (\nabla u_M) = \nabla \cdot \mathbf{M}. \tag{6}$$

The nanotube is discretized into tetrahedral finite elements, according to the Ritz–Galerkin weak formulation.[13] On each node of the finite element mesh, a magnetic moment vector and a magnetic scalar potential is defined. The magnetic scalar potential follows from the magnetostatic boundary value problem. Instead of extending the finite element mesh over a larger region outside the magnet, the boundary element method allows to treat the condition that the potential decays as $1/r$ with distance.[18,19] The space discretization of the LLG equation leads to a system of ordinary differential equations for the magnetic moment at the nodes of the finite element mesh. The equations are coupled by the exchange field and by the magnetostatic field. For time integration, we use an implicit time integration scheme with automatic time step control.[20,21] The $Ni_{80}Fe_{20}$ Permalloy nanotube studied in this work had the following dimensions: external radius of 250 nm, inner radius of 200 nm, and 500 nm length. The intrinsic magnetic properties considered for this nanotube were $J_s = 1.1$ T, $A = 1.3 \times 10^{-11}$ J/m and $K_u = 0$ J/m^3, together with a damping factor of $\alpha = 0.2$. These properties correspond to the Permalloy Ni:Fe ratio which shows vanishing anisotropy values[11,22] and thus, excellent soft magnetic properties. The current carrier model (cylinder of radius 190 and 900 nm length) simulates an applied magnetic field as an alternating circumferential magnetic field h_{ac} by means of an ac current I_{ac}, which in turn was generated as a sin (ωt) signal with $\omega = 2\pi f$ (f= frequency in Hertz, within the range 250 MHz–10 GHz) and I_{rms} values between $(1/\sqrt{2})$ and $(10/\sqrt{2})$ mA, which correspond to h_{rms} fields between 0.45 and 4.5 kA/m on the nanotube´s external surface. Relative circular magnetization M_ϕ curves, with M_ϕ = (magnetization projection)/(saturation magnetization), as a function of h_{ac} were calculated as the projection of the magnetization onto the circumferential applied magnetic field. The DW propagation along the nanotube length produced by h_{ac} was quantified by means of the DW speed v_{DW}, which in turn was determined from cinematic DW-position vs time plots [DW(t)]. These cinematic DW(t) curves were calculated by considering that the relative circular magnetization at any time t_i, $M_\phi(t_i)$, is determined by the DW position $x(t_i)$ along the tube length, since any DW displacement from its initial position (t_0) represent a magnetization variation ΔM_ϕ. Therefore, at t_i, the proportion between $x(t_i)$ and $M_\phi(t_i)$ is given by

$$x(t_i) = \frac{\Delta x}{\Delta M_\phi} M_\phi(t_i), \tag{7}$$

where $\Delta x = x(t_f) - x(t_0)$ and $\Delta M_\phi = M_\phi(t_f) - M_\phi(t_0)$ for an arbitrary final time t_f. The DW position $x(t_i)$ along the nanotube length is determined from the corresponding magnetization distribution calculated at t_i. At the beginning of each DW(t) plot, a nonlinear behavior was observed, which reflects an accelerated DW motion. After a period of about 0.1 T (where $1/T$ is the frequency of the ac applied field) the cinematic DW(t) curve was found to follow a linear trend [just before the first DW(t) maximum] from which v_{DW} was computed.

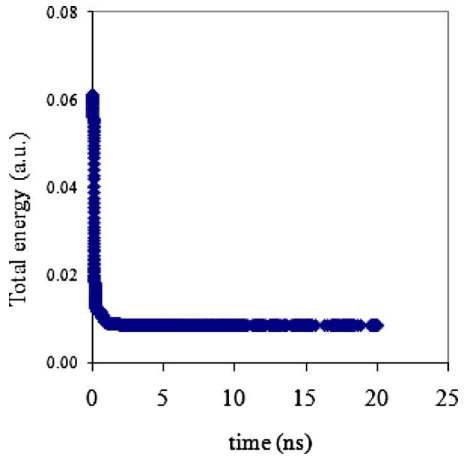

FIG. 1. (Color online) Total energy as a function of time for the $Ni_{80}Fe_{20}$ Permalloy nanotube.

III. RESULTS AND DISCUSSION

The equilibrium configuration of the nanotube was determined from an initially saturated state along the nanotube main axis, using a relaxation time of 20 ns for micromagnetic calculations. After 5 ns, no variations in the total energy were observed (Fig. 1). The equilibrium magnetization distribution consisted of two circular domain regions saturated in opposite direction and separated by a DW, as it is shown in Fig. 2(a). The DW original position was around the center of the nanotube´s axial length, showing a structure corre-

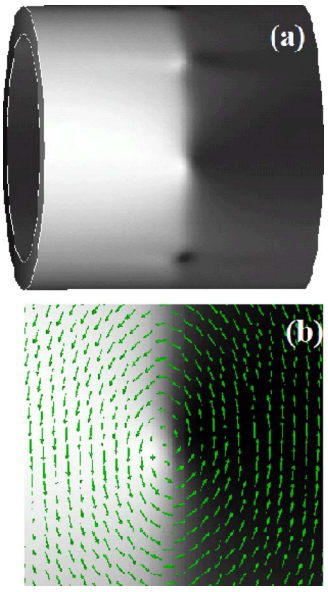

FIG. 2. (Color online) (a) Equilibrium magnetization for the $Ni_{80}Fe_{20}$ nanotube showing a cross-tie type DW separating two domain regions oriented in opposite sense: upwards (dark side) and downwards (light side). (b) A detail of the DW vortex structure.

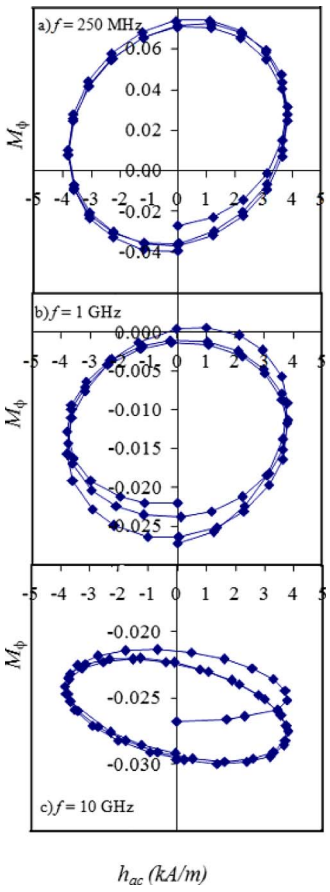

FIG. 3. (Color online) Relative circular magnetization M_ϕ as a function of h_{ac} at various frequency values and for $h_{rms}=(1/\sqrt{2})3.82$ kA/m.

sponding to a cross-tie wall, i.e., comprising a chain of vortices circumferentially arranged, for which Fig. 2(b) displays one vortex structure in detail. This kind of DW has been reported also for Permalloy magnetic thin films[23] and for similar nanotubes.[11,12] The DW width was found to be 30 nm, which is in excellent agreement with the minimum value observed in Ref. 23. Once the DW formation was confirmed, the application of circumferential magnetic fields resulted in an oscillating DW motion whose dynamic characteristics are described in detail in the following.

A. $f=250$ MHz

The relative circular magnetization $M_\phi(h_{ac})$ plot for $h_{rms}=2.7$ kA/m is displayed in Fig. 3(a) showing an oscillating character, with an initial M_ϕ of −0.027. This nonzero value reflects a slightly asymmetrical initial circular magnetization distribution and thus, an original DW location slightly out of the middle nanotube position; in fact, this initial position was determined as being of 258 nm. After the first half cycle of h_{ac}, M_ϕ goes through a maximum value of 0.073 as a consequence of the DW displacement from its original position along the nanotube length. With increasing time [each point of M_ϕ (h_{ac}) is also time dependent], h_{ac} becomes negative and, upon completion of the first cycle, M_ϕ decreases to a preliminary minimum value of −0.035 as the DW moves back to a position on the opposite side of the initial displacement. This position does not coincide with the

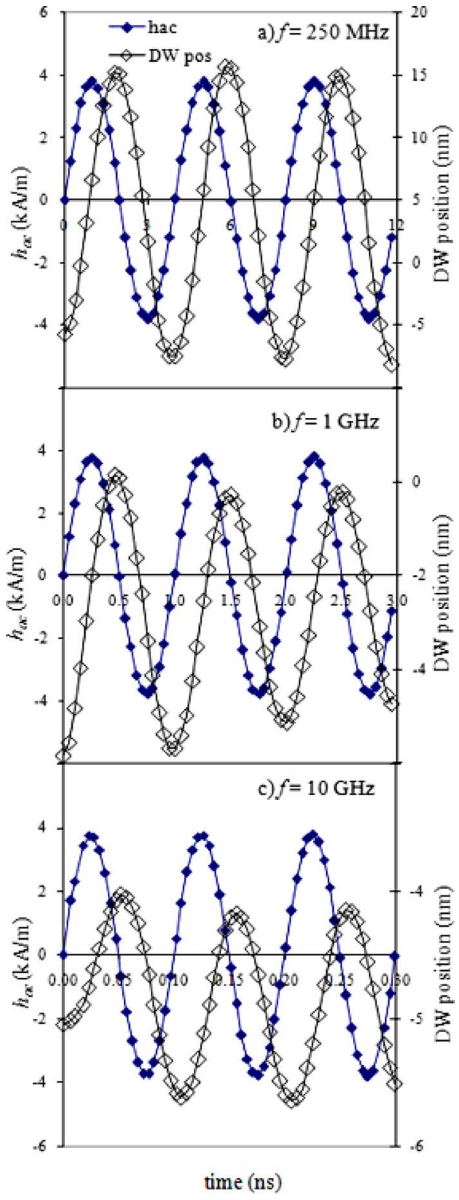

FIG. 4. (Color online) Cinematic DW(t) and $h_{ac}(t)$ curves for the $Ni_{80}Fe_{20}$ nanotube at various frequencies and $h_{rms}=(1/\sqrt{2})3.82$ kA/m.

original one, as it is evidenced by the hysteretic character of the $M_\phi(h_{ac})$ plot. After three periods, the relative circular magnetization reaches a final position, leaving the nanotube in a remanence state of $M_\phi=-0.039$. The corresponding cinematic DW(t) curve together with h_{ac} as a function of time are shown in Fig. 4(a), for which an out-of-phase oscillating DW motion is manifested. The DW oscillation exhibited the same frequency of $h_{ac}(t)$. The phase shift ϕ_N (normalized to T) was determined as 0.21, while the peak-to-peak amplitude of oscillation A_{DW} was of 21 nm. In general, ϕ_N values exhibited small fluctuations around 0.21 (with a standard deviation of 0.02) upon h_{rms} variation, while A_{DW} showed a linear increase between 3 and 36 nm for the h_{rms} interval 0.45–4.5 kA/m. The initial DW position is not at zero, which is congruent with $M_\phi(0)\neq 0$. Similar oscillating DW motions were observed for all h_{rms} values, even for applied fields as low as 0.45 kA/m. Additionally, the DW speed was established as 16.0 m/s from the initial linear portion of the

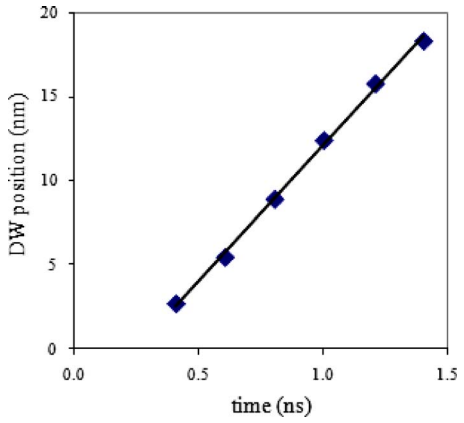

FIG. 5. (Color online) Initial portion of the cinematic DW(t) curve for f =250 MHz and h_{rms}=2.7 kA/m. The straight line corresponds to a linear fitting with R^2=0.999.

cinematic DW(t) displayed in Fig. 5. Further variation of h_{rms} resulted in a linear behavior for the v_{DW} (h_{rms}) plot, as it is shown in Fig. 6, for which the following equation was determined after linear fitting: v_{DW} =0.0061 m^2/s A h_{rms}−1.011 m/s.

B. f=1 GHz

For this frequency, again, oscillating circular magnetization for various h_{rms} values were observed, as it is shown for instance in Fig. 3(b) for the M_ϕ (h_{ac}) plot at h_{rms} =2.7 kA/m. The same initial relative circular magnetization value was observed (−0.027) but, a significantly reduced M_ϕ maximum of just 0.0005 (in comparison with the previous maximum at f=250 MHz) was recorded. This reduction in the ac magnetization also yields to minor DW amplitudes of oscillation, as it is exhibited in Fig. 4(b), for which A_{DW} is only of 6.0 nm with the wavering DW motion occurring on the same side of the nanotube, i.e., the DW displacement does not cross beyond the initial reference position. Moreover, the out-of-phase character of the oscillating motion is also evidenced in Fig. 4(b), with a normalized phase shift of ϕ_N=0.190. In general, ϕ_N values exhibited small fluctuations around 0.190 (with a standard deviation of 0.005) upon h_{rms} variation, while A_{DW} showed a linear increase between 5 and 12 nm for the h_{rms} interval 0.45–4.5 kA/m. On the other hand, v_{DW} as a function of h_{rms} showed also a linear trend (Fig. 6) with enhanced values (respect to those observed at the previous f) which in turn leads to the reduced A_{DW} observed. The following equation was determined after linear fitting: v_{DW}=0.0077 m^2/s A h_{rms}−1.300 m/s.

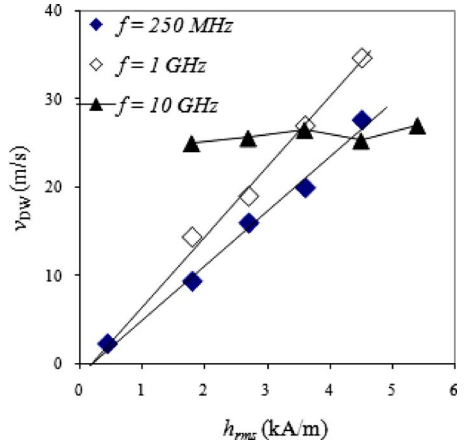

FIG. 6. (Color online) DW speed as a function of h_{rms} and of variable frequency. The straight lines corresponds to linear fittings with at least R^2 =0.99.

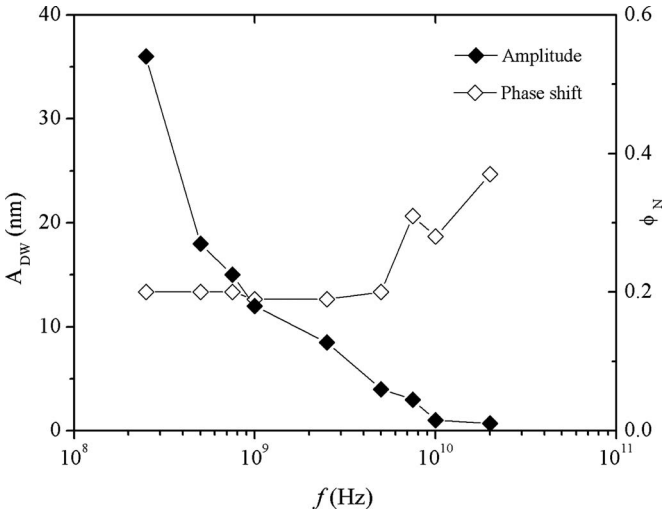

FIG. 7. Normalized (respect to each period) phase shift ϕ_N and DW amplitude of oscillation (for h_{rms}=4.5 kA/m) as a function of the applied field frequency f. The solid lines are a guide for the eyes only.

C. f=10 GHz

At this frequency, a significantly attenuated oscillating circular magnetization is still present, as it is shown, for example, in Fig. 3(c), for which M_ϕ fluctuations of only 0.0053 are visible for h_{rms}=2.7 kA/m. The A_{DW} resulted of just 1 nm for the out-of-phase DW(t) curve with ϕ_N=0.29 [Fig. 4(c)]. This time, ϕ_N showed an enhanced average value of 0.26 (respect to previous f, with a standard deviation of 0.01) upon h_{rms} variation, while A_{DW} displayed a constant value of 1 nm for the considered h_{rms} interval of 0.45–4.5 kA/m. In addition, the v_{DW} (h_{rms}) curve also resulted in a constant tendency around 25 m/s (Fig. 6).

D. Further increase in frequency calculations

Figure 7 exhibits the frequency dependence of ϕ_N and the amplitude A_{DW} for a constant h_{rms} value of 4.5 kA/m. In contrast to the shallow effect of variable h_{rms} on ϕ_N, by increasing the frequency, the normalized phase shift shows an enlargement effect beyond f=5 GHz, with a previous constant trend around 0.20. On the other hand, A_{DW} decreases in a monotonous manner with increasing f, exhibiting negligible values from f=10 GHz, which strongly suggests that the DW motion is damped at this frequency. In addition, the DW speed as a function of f is depicted in Fig. 8 displaying a general increasing tendency with raising f up to 2.5 GHz, followed by a rough constant value up to 7.5, after which a significant drop at f=10 GHz is manifested, giving further support to the assumption of a damped DW displacement at this frequency.

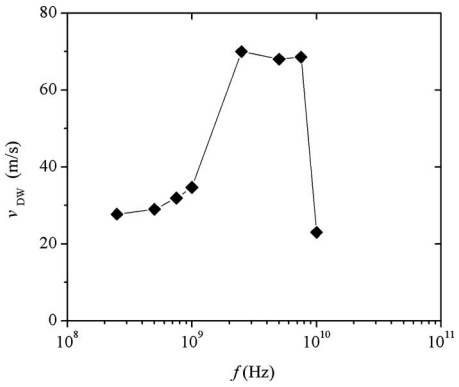

FIG. 8. The DW speed v_{DW} as a function of the applied field frequency for h_{rms}=4.5 kA/m. The solid line is a guide for the eyes only.

In order to clarify the physical meaning of the dynamic parameters obtained for the DW speed as a function of h_{rms}, we should consider the response of a DW under the effect of an external magnetic field $he^{i\omega t}$ (where $i=\sqrt{-1}$ and $\omega=2\pi f$ is the angular frequency), which can be described in a first approximation by the following classical equation of motion:

$$\beta\dot{x} + \alpha_w x = 2\mu_o M_s he^{i\omega t}, \tag{8}$$

where β is the viscous damping parameter, α_ω is the restoring parameter, and M_s is the magnetization saturation. From this expression, the steady-state DW velocity can be resolved as (considering $\beta\omega \gg \alpha_\omega$)

$$v_{DW} = \left(\frac{2\mu_o M_s}{\beta}\right)(h - h_o), \tag{9}$$

where $(2\mu_o M_s/\beta)$ is known as the DW mobility μ_{ob} and h_o corresponds to the propagation field, i.e., the minimum field necessary to begin the DW motion. For the present case, it is clear that the nanotube DW speed as a function of h_{rms} follows Eq. (9) for f=250 MHz and 1 GHz (Fig. 6), as it is expected for typical soft magnetic materials[22,24] and as it has been reported for similar cross-tie DW in nanotubes[25,26] and for DW of different shape than Bloch walls.[27,28] From Eq. (9) it is possible to establish the parameters μ_{ob}, h_o, and β for the Permalloy nanotube of interest as it is shown in Table I.

The β values determined for both frequencies resulted similar to the eddy-current contribution β_e to the viscous damping reported experimentally for Ni-Fe polycrystalline wires [β_e=450 kg/sm^2 (Ref. 27)]. Although being clearly different Permalloy structures (in shape and size), it is interesting to notice that according to present results, an increasing tendency of β with reducing f would be expected and thus, a better matching of β values for frequencies low enough would arise. This is in accordance with the intrinsic character of β, which in fact comprises also a spin relaxation β_r contribution proportional to the material anisotropy constant[27] and thus, being nil for the assumed Permalloy composition.[22,24] In addition, it is worth noticing that the propagation field values found here are also comparable to those measured experimentally in equivalent Ni–Fe nanowires (h_o=400–800 A/m, see Refs 9 and 10) with the additional difference of using simple ac currents rather than spin polarized ones. This implies that the use of nanotubes would be feasible for the manipulation of magnetic DWs because of the low magnetic fields and the type of currents required, and thus, rendering this nanostructures as probable candidates for nanoelectronic devices operating at high frequencies.

TABLE I. Dynamic parameters for DW motion for the Permalloy nanotube.

f (Hz)	μ_{ob} (m^2/sA)	h_o (A/m)	β (kg/sm^2)
250×10^6	0.0061	166	360
1×10^9	0.0077	168	285

IV. CONCLUSION

DW displacement was observed in $Ni_{80}Fe_{20}$ Permalloy nanotubes for propagation fields as low as 166 mA and frequencies of up to 10 GHz. The Oscillating DW motion was found to be out of phase (respect to h_{ac}), with the normalized phase shift being independent of h_{rms} and frequency dependent for $f>5$ GHz.

ACKNOWLEDGMENT

I.B. acknowledges the grant of a sabbatical scholarship from DGAPA-UNAM, Mexico.

[1] N. Wang, T. O'Donnell, S. Roy, P. McCloskey, and C. O. Mathuna, J. Magn. Magn. Mater. **316**, e233 (2007).
[2] Y. Zhuang, M. Vroubel, B. Rejaei, and J. N. Burghartz, Solid-State Electron. **51**, 405 (2007).
[3] J. Y. Park and M. G. Allen, J. Micromech. Microeng. **8**, 307 (1998).
[4] C. Thirion, W. Wernsdorfer, and D. Mailly, Nat. Mater. **2**, 524 (2003).
[5] T. Moriyama, R. Cao, J. Q. Xiao, J. Lu, X. R. Wang, Q. Wen, and H. W. Zhang, Appl. Phys. Lett. **90**, 152503 (2007).
[6] D. A. Allwood, G. Xiong, C. C. Faulkner, D. Atkinson, D. Petit, and R. P. Cowburn, Science **309**, 1688 (2005).
[7] G. S. D. Beach, C. Nistor, C. Knutson, M. Tsoi, and J. L. Erskine, Nat. Mater. **4**, 741 (2005).
[8] R. Varga, A. Zhukov, V. Zhukova, J. M. Blanco, and J. Gonzalez, Phys. Rev. B **76**, 132406 (2007).
[9] L. Thomas, M. Hayashi, X. Jiang, R. Moriya, C. Rettner, and S. S. P. Parkin, Nature (London) **443**, 197 (2006).
[10] L. Thomas, M. Hayashi, X. Jiang, R. Moriya, C. Rettner, and S. S. P. Parkin, Science **315**, 1553 (2007).
[11] J. Lee, D. Suess, T. Schrefl, K. H. Oh, and J. Fidler, J. Magn. Magn. Mater. **310**, 2445 (2007).
[12] J. Escrig, P. Landeros, D. Altbir, E. E. Vogel, and P. Vargas, J. Magn. Magn. Mater. **308**, 233 (2007).
[13] J. Fidler and T. Schrefl, J. Phys. D **33**, R135 (2000).
[14] J. D. Jackson, *Classical Electrodynamics* (Wiley, New York, 1998).
[15] O. Ertl, G. Hrkac, D. Suess, M. Kirschner, F. Dorfbauer, J. Fidler, and T. Schrefl, J. Appl. Phys. **99**, 08S303 (2006).
[16] S. Pissanetzky, IEEE Trans. Magn. **29**, 1282 (1993).
[17] D. A. Lindholm, IEEE Trans. Magn. **20**, 2025 (1984).
[18] D. R. Fredkin and T. R. Koehler, IEEE Trans. Magn. **26**, 415 (1990).
[19] T. R. Koehler, Physica B (Amsterdam) **233**, 302 (1997).
[20] G. Hrkac, T. Schrefl, O. Ertl, D. Suess, M. Kirschner, F. Dorfbauer, and J. Fidler, IEEE Trans. Magn. **41**, 3097 (2005).
[21] G. Hrkac, T. Schrefl, O.Ertl, D. Suess, M. Kirschner, F. Dorfbauer, and J. Fidler, J. Appl. Phys. **97**, 10E311 (2005).
[22] R. C. O'Handley, *Modern Magnetic Materials: Principles and Applications* (Wiley, New York, 2000).
[23] R. Ploessl, J. N. Chapman, A. M. Thompson, J. Zweck, and H. Hoffmann, J. Appl. Phys. **73**, 2447 (1993).

[24]S. Chikazumi, *Physics of Ferromagnetism*, 2nd ed. (Clarendons, Oxford, 1997).
[25]H. Forster, T. Schrefl, W. Scholz, D. Suess, V. Tsiantos, and J. Fidler, J. Magn. Magn. Mater. **249**, 181 (2002).
[26]R. Wieser, U. Nowak, and K. D. Usadel, Phys. Rev. B **69**, 064401 (2004).
[27]R. C. O'Handley, J. Appl. Phys. **46**, 4996 (1975).
[28]D. X. Chen, N. M. Dempsey, M. Vazquez, and A. Hernando, IEEE Trans. Magn. **31**, 781 (1995).